Multifunctional Amino Acid Derivative Coordination Compounds: Novel Contrast Agent and Luminescence Materials

Estitxu Echenique-Errandonea,[a] Sara Rojas,[b] Ana M. Ortuño,[c] Javier Cepeda,[a] Pedro Ramos-Cabrer,[d] Íñigo J. Vitórica-Yrezábal,[b] Juan M. Cuerva,[c] José M. Seco,*[a] and Antonio Rodríguez-Diéguez*[b]

In this work a family of multidimensional (2-(1H-tetrazol-5-yl)ethyl) amino acid coordination compounds have been synthesized and thoroughly characterized. For this purpose, glycine, valine, phenylalanine and tyrosine have been selected as starting amino acids and Mn^{2+}, Zn^{2+} and Cd^{2+} as metallic nodes. From one side, for Mn^{2+} based dimer magnetic resonance imaging studies have been conducted, prompted by the number and disposition of the coordinated water molecules

and taking into consideration the promising future of manganese-based coordination compounds as bio-compatible substitutes to conventional Gd based contrast agents. From another side, d^{10} block metal-based complexes allowed exploring photoluminescence properties derived by in situ synthesized ligands. Finally, amino acid preserved structural chirality allowed us to examine chiroptical properties, particularly focusing on circularly polarized luminescence.

Introduction

In the synthesis of novel coordination compounds in situ metal/ligand reaction is presented as a very important approach for organic and coordination chemistry; traditionally, pre-synthesised commercially obtained ligands and metal ions in the form of metallic salts have been the source for the synthesis of novel coordination complexes. Nonetheless, recently, in situ ligand synthesis appears as an appealing synthetic procedure, particularly for the crystal engineering field since it allows providing not only very stable materials, but also products with limited accessibility or not easily obtained through conventional

methods. In this procedure, conventional ligands are substituted by precursors that undergo a transformation and coordinate to metals to produce single crystals of the desired product.[1,2] Generally, for the synthesis of coordination compounds with extended dimensionality, solvothermal routes have allowed featuring chemical reactions at high temperature and pressure conditions yielding crystalline coordination complexes. Among in situ synthesised ligands, Demko-Sharpeless [2 + 3] cycloaddition reaction[3–5] is presented as an easy-handling alternative for the synthesis of tetrazole derivate ligands by reaction of organonitriles with metal azides (Scheme S1 in the ESI),[6,7] as for instance in the synthesis of [[2-(5-tetrazolyl)ethyl]amino]acetic acid.[8]

In this work, our main goal will be the synthesis of novel luminescent chiral in situ generated tetrazole-derivative amino acid based coordination compounds as novel imaging agents. In situ synthesised coordination compounds will derive by the cycloaddition of cyanoethylated amino acids with sodium azide according to the procedure described by Demko-Sharpeless.[5] For that, amino acids have been used as initial precursors and cyanoethyl functionalization has been previously carried out before tetrazolate transformation.[6,9–11] Amino acids are molecules that contain both amino and carboxylic functionalities and are the monomers in protein synthesis, in other words, the building blocks of life.[4] Tetrazoles are known to be precursors in multiple nitrogen containing heterocycles and are broadly investigated for many medical applications in diverse areas.[4,12–16] Because of their multifunctionality, many examples of several coordination compounds and MOFs have been reported in the literature so far.[17–20] In fact, the combination of amino acids with tetrazoles not only derives in ligands with multiple binding sites what promotes stable tridentate structures when coordinated to metal centres, but also tetrazole

[a] Dr. E. Echenique-Errandonea, Dr. J. Cepeda, Dr. J. M. Seco
Department of Applied Chemistry, Faculty of Chemistry
University of Basque Country/Euskal Herriko Unibertsitatea (UPV/EHU)
20018, Donostia, Spain
E-mail: josemanuel.seco@ehu.es

[b] Dra. S. Rojas, Dr. Í. J. Vitórica-Yrezábal, Prof. A. Rodríguez-Diéguez
Department of Inorganic Chemistry
University of Granada
C/ Severo Ochoa s/n, 18071, Granada, Spain
E-mail: antonio5@ugr.es

[c] Dr. A. M. Ortuño, Prof. J. M. Cuerva
Department of Inorganic Chemistry
University of Granada
C/ Severo Ochoa s/n, 18071, Granada, Spain

[d] Dr. P. Ramos-Cabrer
Magnetic Resonance Imaging Laboratory
CIC biomaGUNE
20014 Donostia-San Sebastián, Spain

Chemistry–A European Journal

Research Article
doi.org/10.1002/chem.202304146

Chemistry Europe
European Chemical
Societies Publishing

functionality enhances light absorption promoting better emissive capacity of the synthesised materials.

In diagnosis, when conditions, animalities, injuries or abnormalities such as damaged cellular tissue, tumours, organ injuries, among others need to be locally detected, magnetic resonance imaging (MRI) and fluorescence imaging are a powerful non-invasive techniques that allows focalised and temporal resolution and offers unique diagnostic information avoiding the need for harmful invasive interventions such as biopsies.[21] Concretely, MRI is based on nuclear spins magnetization and makes use of energies in the radio frequency range to alter the alignment of the magnetization of nuclear spin, most commonly belonging to water molecules, thus causing these hydrogen nuclei to produce a detectable rotational magnetic field.[22] Contrast agents can be classified regarding the mechanism of contrast generation. Four major subgroups are differentiated in function depending on their behaviour under the effect of a magnetic field.[23] Contrast agents that shorten both longitudinal and transverse relaxation times to approximately the same degree are called T_1-contrast agents. Agents that shorten transverse relaxation times to a much greater extent than longitudinal relaxation times are called T_2-contrast agents.[24]

The parameter that measures the effect of contrast agents is relaxativity and it is commonly measured in $mM^{-1}s^{-1}$ units. The final value of the relaxativity is a complex mixture of effects, including the molecular structure of the contrast agent (CA) and/or kinetics of the complex with the water molecules. As a general strategy, a signal enhancement is obtained by maximizing the number of unpaired electrons of CA, in addition to increasing the number of accessible water molecules in the inner sphere of the complex and minimizing the distance between metal ion and water protons, which enables signal increment.[25]

Several key elements must be taken into consideration for a successful design of a MRI CA: relaxativity, toxicity, stability, biodistribution and pharmacokinetics are among them. Because the potential *in vivo* use of the CAs, they should have minimal risk of toxicity and be stable in application media. This is why it is relatively common that CAs generally consist of as chelated metal complexes since they allow masking of the potential toxicity of free metal ions. Another key element is CAs' pharmacokinetic; which involves absorption, distribution, metabolism and excretion, this last step is described as the removal process of MRI CAs from the body. Although absorption and metabolism have relatively low influence along the aforementioned process, distribution is fundamental as it rules the scope of *in vivo* application of MRI. The pursued objective is to obtain a specific accumulation in the site of interest.[26,27]

In this work, we will focus on paramagnetic contrast agents. They are characterized by having unpaired electrons in the metal orbitals that act as T_1 shortening relaxation pathways in the protons of the water molecules present in the medium. Paramagnetic contrast agents or positive contrast agents are by far the clinically most employed CAs, that increase the MRI

signal coming from the region where the CA is distributed to. In the literature, several examples can be found.[27]

Among T_1 shortening contrast agents, historically, Mn^{2+} has been selected as the first chemical species to demonstrate the paramagnetic contrast enhancement in MRI. The very first MR phantom image published in 1973 by Lauterbur[28] summarizes that $MnSO_4$ was used to create the contrast in the first MR phantom images. Concerning biocompatibility, Mn^{2+} is an essential micronutrient and a cofactor of various enzymes responsible for diverse cellular functions and controls oxidative stress.[26] Nonetheless, in practice, Gd-based MRI CAs have been more extendedly used in clinics and have been heavily relied upon radiologic diagnosis of tissue. However, long-term Gd retention concerns from the point of view of toxicity since it is known that after CA exposure some patients can develop fibrosis.[29] In this work, we have *in situ* synthesized a novel Mn^{2+} based coordination compound and examined it as a possible MRI contrast agent. Additionally, to analyse the photoluminescent behaviour, tetrazole derivative amino acid ligands and biologically acceptable d^{10} block metals have been selected as metal sources. The closed-shell configuration of metals disables possible potential quenching processes derived from d-d transitions permitting luminescent emission, consequently, the lowest energy excited states of their complexes are mainly for a ligand centred (LC) or/and ligand to ligand charge transfer (LLCT) nature.[30–32] Ligand centred emission processes are favoured by extended conjugated systems. Tetrazole derivative *in situ* synthesised amino acid ligands will display such aromaticity being adequate candidates for exhibiting long lasting luminescent properties.[33]

Finally, we further wanted to exploit another functionality of our materials and motivated by the preserved chirality of the amino acid precursors in synthesised compounds, for this reason, we have investigated the ability of our materials to display differential absorption of right- and left-circularly polarized light.[34] Circularly polarized luminescence can be employed as the source of information about chiral substances (conformation information) and finds application in diverse areas from information processing,[35] OLED[36] to bioimaging.[37] Exploring new approaches to construct CPL active materials with maximum g_{lum} values is if of great importance.

All of the above, a new family of tetrazolyl amino acid derived coordination compounds have been synthesised and characterized for finding application in molecular imaging, photoluminescence and chiroptical applications.

Results and Discussion

Structural Characterization

Single crystal studies revealed that compound **1** (Mn_gly) exhibits the following formula $[Mn_2L^1_2(H_2O)_4]\cdot H_2O$, where $H_2L^1 =$ (2-(1H-tetrazol-5-yl)ethyl)glycine. It was *in situ* synthesised by [2+3] cycloaddition of sodium azide to N-(cyanoethyl)glycine and crystallizes in the monoclinic $P2_1/c$ space group. The asymmetric

Chemistry–A European Journal

Research Article
doi.org/10.1002/chem.202304146

Chemistry
Europe
European Chemical
Societies Publishing

unit of this dimeric entity is composed of one ligand molecule and one metallic centre (Figure 1a).

The coordination environment is completed by the coordination of two water molecules, and a crystallization water molecule. Mn1 atom presents a hexacoordinated MnN_3O_3 environment composed by the coordination of three nitrogen atoms belonging two of them to a tetrazolyl moiety (from two different ligands) and the remaining nitrogen corresponding to the amino group of the amino acid precursor. One oxygen atom corresponds to a monodentate carboxylate moiety of the organic ligand and the remaining two oxygen atoms to two coordinated water molecules. Continuous shape measurements (CShMs)[38] revealed that Mn1 builds octahedral polyhedron (Table S1). Growing the asymmetric unit, it can be seen that the dimeric structure presents hydrogen bonding governed by supramolecular interactions (Figure 1b).

Single-crystal X-ray crystallographic studies carried out on isostructural enantiomeric pairs with the formula $[ZnL^2]_n$ where H_2L^2 is 2-(1H-tetrazol-5-yl)ethyl)-L-valine or (2-(1H-tetrazol-5-yl)ethyl)-D-valine generated by [2+3] cycloaddition of sodium azide to the corresponding N-(cyanoethyl)-L or D-valine, yields respectively compounds Zn–L_val (**2**) and Zn–D_val (**3**). The enantiomeric pairs revealed three dimensional MOFs that crystalise in the orthorhombic $P2_12_12_1$ space group.

The asymmetric unit of **2** and **3** is comprised of a doubly deprotonated ligand (carboxylate and tetrazolate) molecule and one metallic centre. The organic linker, 2-(1H-tetrazol-5-yl)ethyl)valine coordinates to the Zn^{2+} through the oxygen atom of the carboxylate moiety as well as through two nitrogen atoms, one belonging to the amino group and the other belonging to the tetrazolate ring of the amino acid derivative.

Zn1 presents a $[ZnN_3O_2]$ coordination environment in compounds **2** and **3** composed of the *syn-anti* monodentate coordination of two oxygen atoms belonging to the carboxylate moieties of two ligands molecules, two nitrogen atoms of a tetrazolate moiety again from adjacent ligands as well as from the coordination of the nitrogen atom belonging to the amino group of the amino acid derivative. Continuous shape measurements (CShMs)[38] revealed that Zn1 build a spherical square pyramid (SPY-5) polyhedron (Table S2).

The analysis of the topology through TOPOS Pro software[39] reveals that compounds **2** and **3** possess a 6-c uninodal net with $(3^3 \cdot 5^9 \cdot 6^3)$ point symbol and **lcy** topology. Although the structure expands in three dimensions (Figure 2) the growth of the structure does not have solvent accessible volume accord-
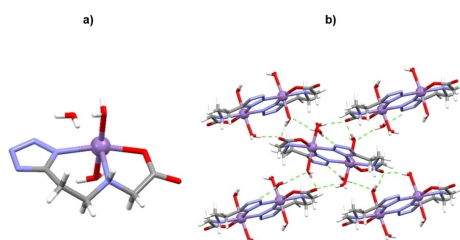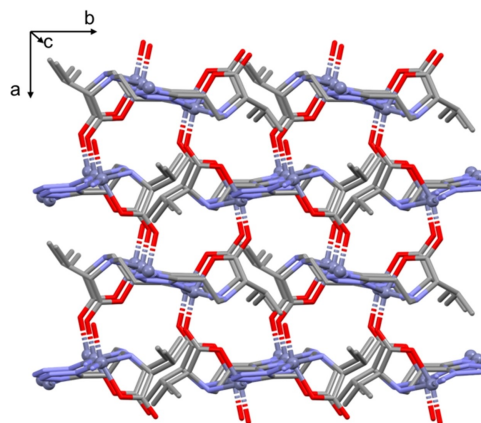

Figure 2. View of the crystal packing of compound **2** along crystallographic *c* axis.

ing to the geometrical calculations performed with the PLATON program.

Single-crystal X-ray crystallographic studies undertaken on isostructural enantiomeric pairs with the formula $[ZnL^3]_n$ where H_2L^3 is 2-(1H-tetrazol-5-yl)ethyl)-L-phenylalanine or (2-(1H-tetrazol-5-yl)ethyl)-D-phenylalanine which were derived by *in situ* [2+3] cycloaddition of sodium azide with the corresponding N-(cyanoethyl)-L or D-phenylalanine, yields respectively compounds Zn–L_phen (**4**) and Zn–D_phen (**5**). Note that good quality single-crystals have been only obtained for compound **5** but due to the isostructural character of compound **4** in the following section compound **5** description will be performed in detail as a representative example of the enantiomeric pair. Compounds **4** and **5** exhibit layered two-dimensional structure (Figure 3) that crystallises in the monoclinic $P2_1$ space group. The asymmetric unit of these compounds is composed of a doubly deprotonated ligand molecule and a Zn^{2+} metallic centre. As for the previous examples, the organic ligand coordinates the metallic centre by means of the carboxylate moiety (in a monodentate way in *syn-anti* disposition to neighbouring metallic centres) and the amino and tetrazole nitrogen atoms.
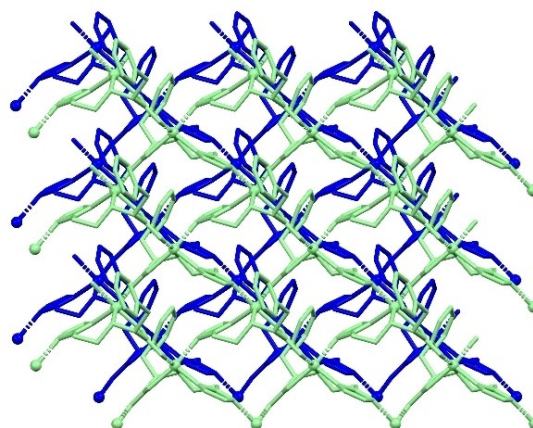

Figure 1. a) Excerpt of the asymmetric unit of compound **1**. **b)** perspective view of the packed dimeric structure where H bonding interactions are shown in dashed green lines.

Figure 3. Perspective view of the packed structure of **4** and **5**.

Zn1 presents a $[ZnN_3O_2]$ coordination environment in compounds **4** and **5** composed of the *syn-anti* monodentate coordination of the oxygens belonging to adjacent carboxylates, in addition to the coordination from the nitrogen of the amino group as well as to two nitrogen atoms from the tetrazolate moiety. Continuous shape measurements (CShMs) reveal that Zn1 build a spherical square pyramid (SPY-5) polyhedron (Table S2). Two-dimensional layered topology performed with TOPOS Pro software exhibits that compounds **4** and **5** display a 3.5-c unimodal net with $(3 \cdot 5^2)(3^2 \cdot 5^3 \cdot 6^4 \cdot 7)$ point symbol and **3,5L50** topology.

To conclude with the structural description, single-crystal X-ray crystallographic studies performed on isostructural enantiomeric pairs with the formula $\{[ZnL^4] \cdot H_2O\}_n$ and $\{[CdL^4] \cdot H_2O\}_n$ where H_2L^4 is 2-(1H-tetrazol-5-yl)ethyl)-L-tyrosine or (2-(1H-tetrazol-5-yl)ethyl)-D-tyrosine *in situ* generated by [2+3] cycloaddition of sodium azide to the corresponding N-(cyanoethyl)-L- or -D-tyrosine, yields respectively two isostructural enantiomeric pairs, in advance, Zn–L_tyr (**6**) and Zn–D_tyr (**7**), Cd–L_tyr (**8**) and Cd–D_tyr (**9**), respectively. Good quality single-crystals have been obtained for Zn^{2+} counterparts, nonetheless, due to the isostructural nature of Cd^{2+} enantiomeric pairs, the crystal description of **6** will be held in advance as a representative example of the isostructural family. Compounds **6–9** exhibit a two-dimensional structure that crystallises in the orthorhombic $P2_12_12_1$ space group. The asymmetric unit of **6–9** is composed of a doubly deprotonated (carboxylate and tetrazolate; note that the phenol group remains unaltered providing intermolecular hydrogen bonds) ligand molecule and a Zn^{2+} metallic centre in addition to a crystallization water molecule.

In resemblance to the previously described structures, 2-(1H-tetrazol-5-yl)ethyl) tyrosinate ligand coordinates the metallic centre from the carboxylate moiety (in a monodentate way in *syn-anti* disposition to adjacent metallic centres) and from the nitrogen's one, belonging to the tetrazolate moieties and the other to the amino group of the amino acid derivative (Figure 4).

Zn1 presents a $[ZnN_3O_2]$ coordination environment in compounds **6–9** composed of the *syn-anti* monodentate coordination of the oxygens belonging to adjacent carboxylates, in add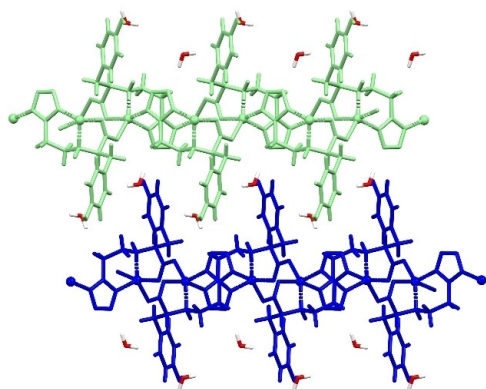ition to the coordination from the nitrogen of the amino group as well as to two nitrogen atoms from the tetrazolate moiety. Continuous shape measurements (CShMs)[38] reveal that Zn1 build a spherical square pyramid (SPY-5) polyhedron (Table S2).

Two-dimensional layered topology performed with TOPOS Pro software exhibits that compounds **6–9** display a 3.7-c unimodal net with $(3 \cdot 5^2)(3^2 \cdot 5^{11} \cdot 6^7 \cdot 7)$ point symbol. Growing the asymmetric unit, it can be seen that the layered structure presents remarkable supramolecular interactions which are governed by hydrogen bonding interactions.

Relaxativity Measurements

To understand how Mn_gly (**1**) performs as a potential contrast agent for MRI, we studied its relaxativity under 1.4 T scanner at Bruker Minispec mq60 working at 37 °C and at 7 T by a Bruker Biospec 70/30 preclinical MRI spectrometer. The former equipment provides the relaxativity of a compound in the clinical field and at body temperature giving an idea of the performance as a potential contrast agent in clinical environments while the latter, provides relaxativity values at a much higher magnetic field, typically used in preclinical research. Relaxativity measurements undertaken in compound **1** were carried out (Figure 5) in ultrapure Milli-Q water media at three different concentrations (1.0 mM, 0.5 mM and 0.1 mM) for both fields (1.4 T and 7 T). In order to characterize these dispersions, and to know how the particles of **1** behave in the aqueous media, dynamic light scattering measurements were performed. Attempts to perform the measurements in the three concentrations revealed that only the intermediate concentration was appropriate, because 1.0 and 0.1 mM are too dilute and too concentrate as to provide a reliable analysis and avoid heterogeneity on the particle size and diffusivity. Several scans were acquired on ultrasonicated dispersions of 0.5 mM, achieving a homogeneous mean hydrodynamic size of about 290 nm (Figure S12). On its part, the dispersion showed a zeta potential of -8.92 mV, a value similar to that found in other Mn(II) complexes[40] that supports the negative charges occupying the surface of the particles in good agreement with the presence of non-bonding carboxylate groups of $(L^1)^{2-}$ ligands of the dimeric entities. Futhermore, an aliquote of the aqueous solution of compound **1** in the 0.5 mM concentration was also analysed by means of liquid chromatography-mass (UHPLC/Q-TOF-MS)
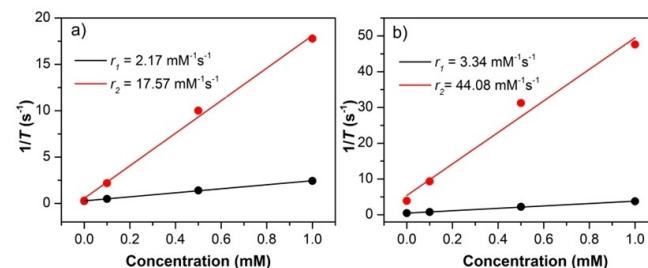

Figure 4. View of packed structure of **6** along *a* axis.

Figure 5. Longitudinal (r_1) and transverse (r_2) relaxativity rate of compound **1** as a function of Mn^{2+} concentration measured in **a)** Minispec at 1.4 T and **b)** in Bruker Biospec 70/30 at 7 T, respectively.

Chemistry–A European Journal

Research Article
doi.org/10.1002/chem.202304146

Chemistry Europe
European Chemical
Societies Publishing

technique in order confirm the integrity of the particles in solution. As shown in Figure S13 of the ESI, the ionized fragments concord well with the expected mass units for a dimeric charged $[Mn_2L^1_2(H_2O)_4]^-$ complex.

Relaxativity is dependent on external parameters among which applied field, temperature and hydration state of the molecule can be highlighted. Regarding applied field, it is known that r_1 relaxativity typically decreases with an increase of the external field while transverse relaxativity, r_2, is static or increases resulting in an increased r_2/r_1 ratio.[41]

This r_2/r_1 ratio classifies a substance working as a T_1 or T_2 contrast agent. Generally, contrast agents with a low r_2/r_1 ratio (<5) are classified as T_1 substances, while agents exhibiting larger ratios (>10) are categorized as T_2 contrast media.[24] The longitudinal (r_1) and transverse (r_2) relaxativity values were calculated from the slope of the plot of $1/T$ vs. [Mn] expressed in mM.

The r_1 value obtained for Mn^{2+} was 2.17 mM^{-1}s^{-1} and 3.34 mM^{-1}s^{-1} at 1.4 T and 7 T, respectively; little below relaxativities found for small Mn^{2+} complexes containing one inner-sphere water molecule which generally exhibit r_1 values of 2.4–3.7 mM^{-1}s^{-1} at 0.47 T and 25 °C[42,43] and comparable to Mangafodipir trinatrium Mn-DPDP ($r_1 = 2.1$ mM^{-1}s^{-1}, 20 °C, 1.5 T[44]), an intravenously administrated CA used to enhance the contrast of the liver and pancreas marketed under the name of Teslascan®.[44] As previously stated, the r_2/r_1 ratio rules a contrast agent potentially working as a T_1 brightening or T_2 endarkening agent and ratios below 5 are categorized as T_1 substances, while agents exhibiting larger ratios (over 10) are classified as T_2 contrast substance. In our studied compound **1**, the ratio r_2/r_1 was 8.1 for 1.4 T and 13.2 for 7 T, working potentially as a T_2 substance. Subsequently, to evaluate the efficiency of compound **1** as a brightening or endarkening contrast agent, T_1 and T_2 weighted-phantom MR images of the complex at three concentrations have been collected. A T_1-weighted image will expect to present water with a shorter relaxation time displaying a brighter image; while in a T_2-weighted image, the shorter T_2 signal, the faster will disappear and thus, the presence of the CA will contribute to destroying signal deriving in a darker image.

In principle, obtained relaxativity values both at 1.4 T and 7 T (Tables S3 and S4, ESI) fields have demonstrated relatively high r_2/r_1 ratios considering **1** behaving as a potential T_2 contrast agent. For the aforementioned measurements, again, analysis was carried out in ultrapure Milli-Q water media at three different concentrations for compound **1** and in 1 mM concentration for MnCl$_2$ which was used as a reference. It would be expected for MnCl$_2$ to display higher r_1 and r_2 values since possibly the number of accessible and interchangeable water molecules in the metal surrounding would be higher in number compared to compound **1**.

At a first sight, taking into consideration T_1 and T_2 weighted-phantom MR images we can appreciate that our contrast agent at 1 mM concentration possesses a slightly brighter contrast ability compared to 1 mM MnCl$_2$ dissolution mainly associated with the coordinated water molecules in the complex's inner-

sphere, leading to the exchange of water molecules with the surrounding water.

Although, T_1-weighted images exhibit that intensity of the image was found to slightly increase with concentration increasing of complex **1** is detectable (see Figure 6, up), T_2-weighted images with increasing concentrations exhibit smaller signal coming in accordance with the behaviour expected for relatively high r_2 values, (concretely of 44 mM^{-1}s^{-1} at 7 T for **1**) as shown in Figure 6 (bottom). Given these results, it can be stated that synthesized compound **1**, which under clinical conditions (1.4 T and 37 °C) has demonstrated an r_1 value of 2.17 mM^{-1}s^{-1}, a relatively high r_2/r_1 ratio of 8.1 along with an efficient negative effect as estimated from the T_2-weighted MR image, could have potential applicability as a novel T_2 negative contrast agent.

Photoluminescence Measurements

Solid-state photoluminescence measurements were conducted in polycrystalline samples to assess emission characteristics and study the influence of the assembling ligands. Note that, due to the equivalent emission of enantiomers, the emission capacity of one enantiomer has been studied as representative of the pair. Synthesised d^{10} metal complexes present extended aromaticity promoted by a poly-heterosubstituted penta-atomic ring; this feature made us think about the possibility of these entities being good candidates for displaying enhanced photoluminescent properties. In addition to that, ligand coordination to metals with fully-filled d orbitals promote structural rigidity, and in consequence, reduces the efficiency of non-radiative pathways yielding increased fluorescent emission. Because of that, d^{10} metal complexes have been broadly studied for applications ranging from fields of sensing to photochemistry, so far.[45,46]

To begin with, the excitation spectrum of Zn_val recorded at 15 K (Figure 7) monitoring at the ligand emission at 394 nm display a broad band ranging from 250–400 nm where a set of transitions are appreciable peaking at 289, 328, 336 and 340 nm, respectively. 15 K emission spectrum of Zn_val has been collected upon excitation at 289 nm. The emission profile consists of a main broad band, from 350 to ca. 650 nm, with the maximum intensity at 445 nm with a set of less intense shoulders peaking at 384, 416 and 463 nm, respectively. The
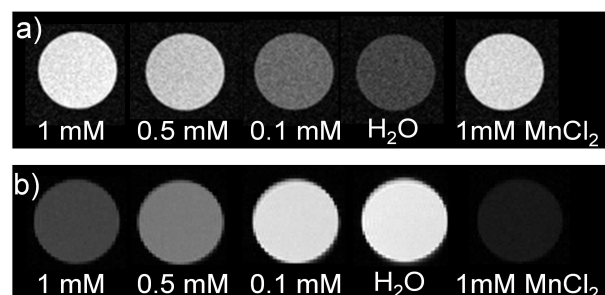

Figure 6. a) T_1-weighted (up) and **b)** T_2-weighted (bottom) phantom MR images of complex **1** and MnCl$_2$ at different concentrations at 7 T.

Chemistry–A European Journal

Research Article
doi.org/10.1002/chem.202304146

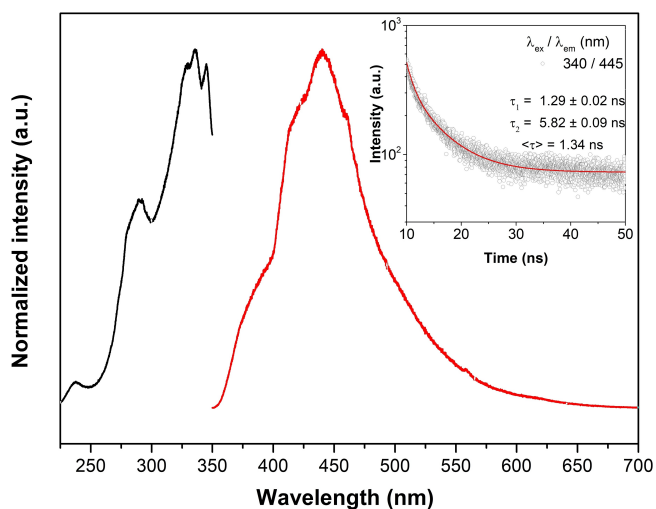**Chemistry Europe**
European Chemical
Societies Publishing

Figure 7. 15 K excitation spectra of Zn_val (black; $\lambda_{Exc.} = 394$ nm) and emission spectra (red) with the excitation fixed at 289 nm. The inset shows the corresponding decay curve monitoring the emission at 445 nm with the excitation selected at 340 nm collected at room temperature; the solid red lines are the best fits using second-order decay functions, $y = y_0 + A_1 \cdot \exp(-x/\tau_1) + A_2 \cdot \exp(-x/\tau_2)$ ($r^2 > 0.999$). The average lifetimes were calculated according to the formula $< \tau > = (A_1\tau_1^2 + A_2\tau_2^2)/(A_1\tau_1 + A_2\tau_2)$.

emission of Zn_val stems from the ligand centred π-π^* electronic transition suggesting that the conjugated ligand is the part contributing to the emission while the Zn^{2+} centre commits to structural rigidity enhancing ligand emissive properties. Zn_Val decay curve recorded at ambient temperature while monitoring the strongest emission at 445 nm under direct excitation at 340 nm (inset of Figure 7), is only properly fitted by a second order exponential function yielding lifetimes of 5.82 ± 0.09 ns and 1.29 ± 0.02 ns with an averaged lifetime of 1.34 ns. It must be noted that the contribution of the longest decay time is significantly higher than the shortest one and that decays shorter than 1 ns can be assessed to lamp pulse.

Emission spectra of Zn_val were performed at different temperatures (15–300 K) selecting the excitation at 289 nm to study temperature induced changes in the emission spectrum (Figure 8). For that, the temperature dependence of the integrated intensity (I_{Zn_Val}) was determined by integrating emission spectra in the range of 350–575 nm. As shown in the thermal behaviour (Figure 8), there is a linear relationship between temperature and emission intensity, following the expected trend by which temperature decrease diminishes the relaxation via non-radiative paths and, thus, it brings an increment in the emission intensity.

Subsequently, the excitation spectrum of Zn_phen recored at 10 K and monitored at the maximum emission at 480 nm shows a broad band, from 275 to 400 nm, with the maximum at 388 nm with a shoulder at 309 nm (Figure 9). The emission spectrum of Zn_phen, collected at 10 K and, excited at 325 nm presents a broad band, from 350 to ca. 750 nm, exhibiting the maximum intensities at 413 nm and 500 nm which is attributed, as for Zn_val analogue, to ligand aromatic π-π^* electronic transition. Zn_phen decay curve recorded at ambient temperature while monitoring the strongest emission at 480 nm under
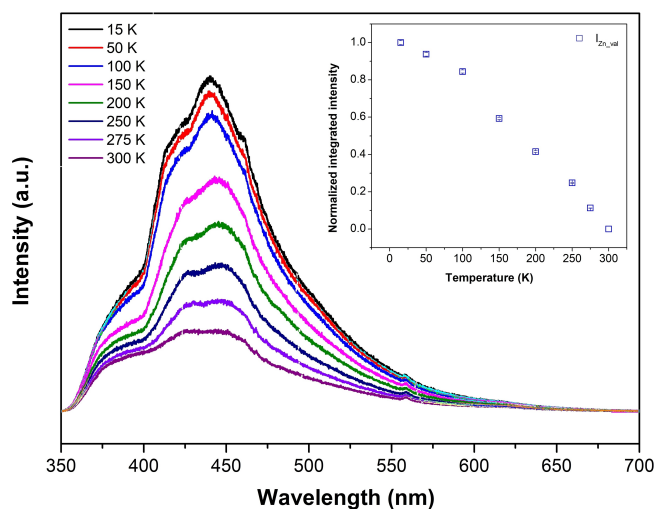

Figure 8. The emission spectra of Zn_val in the 15–300 K range with the excitation selected at 289 nm. Inset: Temperature dependence of $I_{Zn\text{-}val}$ in the same temperature range.
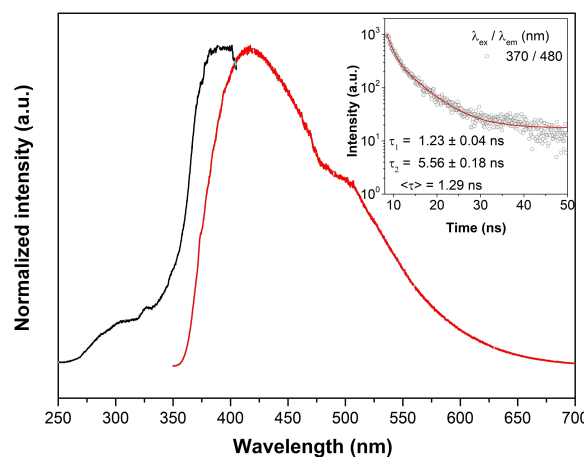

Figure 9. 10 K excitation spectrum of Zn_phen (black; $\lambda_{Exc.} = 552$ nm) and emission spectrum (red) with the excitation fixed at 325 nm. The inset shows the corresponding decay curve monitoring the emission at 480 nm with the excitation selected at 370 nm collected at ambient temperature; the solid red lines are the best fits using second-order decay functions, $y = y_0 + A_1 \cdot \exp(-x/\tau_1) + A_2 \cdot \exp(-x/\tau_2)$ ($r^2 > 0.999$). The average lifetimes were calculated according to the formula $< \tau > = (A_1\tau_1^2 + A_2\tau_2^2)/(A_1\tau_1 + A_2\tau_2)$.

direct excitation at 370 nm (inset of Figure 9), is only properly fitted by a second order exponential function yielding lifetimes of 5.56 ± 0.18 ns and 1.23 ± 0.04 ns with an averaged lifetime of 1.29 ns. It must be noted that the contribution of the longest decay time is significantly larger than the shortest one and that decay times shorter than 1 ns can be assigned to the laser pulse.

To conclude, the emission capacity of isostructural Zn_tyr and Cd_tyr analogues has been studied in detail (Figure 10). The excitation spectrum recored at 10 K of Zn_tyr monitored at the maximum emission at 511 nm shows a broad band, from 275 to 400 nm, with the maximum at 377 nm with a shoulder at 313 nm. On its part, the isostructural Cd_tyr possesses a highly resembling excitation spectrum displaying a broad band
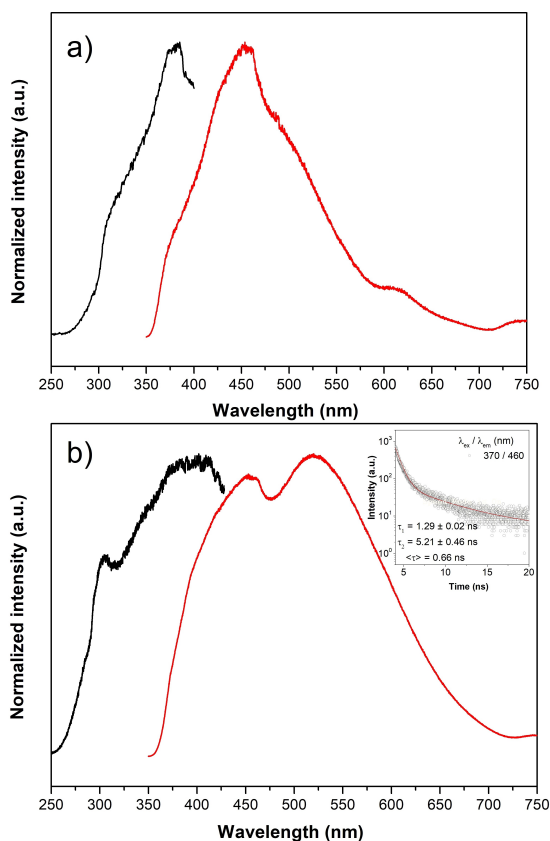
Figure 10. a) 10 K excitation spectrum of Zn_tyr (black; $\lambda_{Exc.} = 511$ nm) and emission spectrum (red) with the excitation fixed at 325 nm. **b)** 10 K excitation spectrum of Cd_tyr (black; $\lambda_{Exc.} = 520$ nm) and emission spectrum (red) with the excitation fixed at 325 nm The inset shows the corresponding decay curve monitoring the emission at 460 nm with the excitation selected at 370 nm collected at ambient temperature; the solid red lines are the best fits using second-order decay functions, $y = y_0 + A_1 \cdot exp(-x/\tau_1) + A_2 \cdot exp(-x/\tau_2)$ ($r^2 > 0.999$). The average lifetimes were calculated according to the formula $<\tau> = (A_1\tau_1^2 + A_2\tau_2^2)/(A_1\tau_1 + A_2\tau_2)$.

located in the range of 250–400 nm and with a well-defined shoulder peaking at 306 nm and 399 nm when excited at 520 nm. The emission spectra of Zn_tyr and Cd_tyr, recorded at 10 K and, excited at 325 nm presents a broad band, from 350 to ca. 750 nm attributed, as for Zn_val analogue, to ligand aromatic π-π^* electronic transition. Nonetheless, it must be noted that Zn_tyr analogue exhibits poorly defined shoulders peaking at 377 and 511 nm with the spectrum maximum located at 452 nm; while the Cd_tyr emission spectrum displays a similar emission pattern with maxima located at the same position, but a higher relative intensity in 519 nm peak concerning 453 nm signal.

Cd_tyr decay curve recorded at room temperature for the strongest emission at 460 nm under direct excitation at 370 nm (inset of Figure 10 b), is only properly fitted by a second order exponential function yielding two lifetimes of 5.21 ± 0.46 ns and 1.29 ± 0.02 ns with an averaged lifetime of 0.66 ns.

Variable temperature emission spectra were performed in Zn_tyr to explore temperature induced changes in the emission spectrum. By integrating the emission spectra in the range of 350–750 nm the corresponding temperature dependence of

the integrated intensity (I_{Zn_tyr}) was calculated. Inset of Figure 11 exhibits a linear relationship dependency among emission intensity and temperature; as it was expected, since it is known that low temperature minimizes kinetic energy of molecules and thus, disables electrons being relaxed from excited states through non-emissive paths.

Chiroptical Properties of MOFs

Circular Dichroism Experiments

Given the chiral nature of the synthesised compounds (**2**–**9**), differential absorption of the right and left circularly polarized light (CD) was investigated as the absolute configuration of homochiral coordination compounds can be confirmed by positive or negative CD signals (Figure 12). For that, the corresponding water suspensions CD spectra were collected
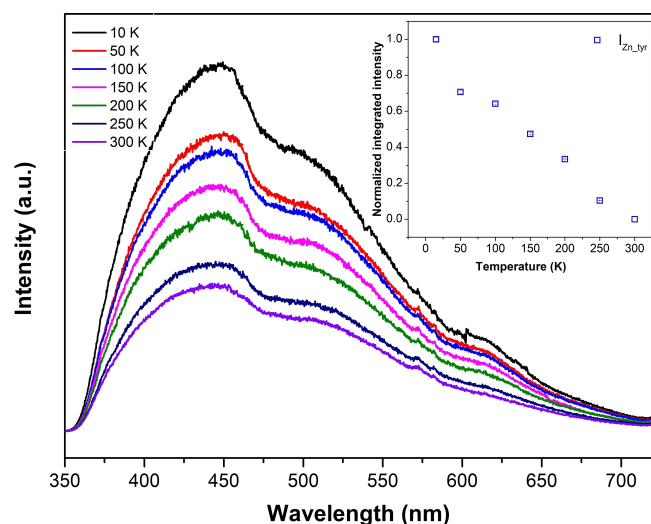

Figure 11. The emission spectra of Zn_tyr in the 15–300 K range with the excitation selected at 325 nm (laser). Inset Temperature dependence of I_{Zn_tyr} in the same temperature range.
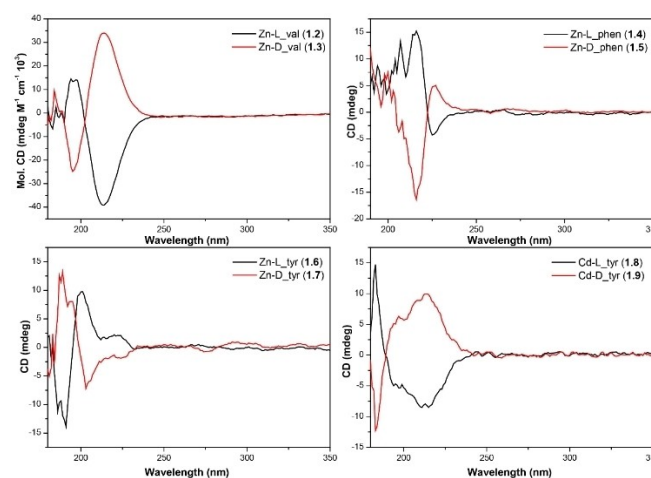

Figure 12. Circular dichroism spectra were recorded for compounds **2**–**9**.

Chemistry–A European Journal

Research Article
doi.org/10.1002/chem.202304146

Chemistry
Europe
European Chemical
Societies Publishing

from each enantiomeric pair according to the procedure detailed in the experimental section. As observed in Figure 12, spectra of enantiomeric compounds are mirror-symmetric images indicating in all cases the formation of enantiopure samples.

When CD spectra of each pair are analysed in detail, Zn–L_val (**2**) and Zn–D_val (**3**) spectra exhibit several bands with maxima at 183, 196 and 213 nm with alternating Cotton effects. Compounds Zn–L_phen (**4**) and Zn–D_phen (**5**) peak at 194, 207, 217, 226 and 267 nm. Compounds Zn–L_tyr (**6**) and Zn–D_tyr (**7**) display a set of bands located at 180, 186, 191, 202, 236 and 287 nm. Finally, Compounds Cd–L_tyr (**8**) and Cd-D_tyr (**9**) exhibit three main bands at 183, 213 and 230 nm, with alternating Cotton effects for all previously described compounds (**4**-**9**). Note that, despite the isostructural nature of compounds Zn–L_tyr (**6**) and Zn–D_tyr (**7**) concerning Cd–L_tyr (**8**) and Cd–D_tyr (**9**) CD spectra exhibit slightly different shape which is due to the data collection parameters. Nonetheless, the maxima peak at a similar wavelength. In all cases, CD absorption bands are present in the corresponding UV-Vis spectra in compounds (**2**–**9**).

Circularly Polarized Luminescence Experiments

In the present work, circularly polarized luminescence spectra have been collected in suspension for left-handed and right-handed enantiomers of compounds Zn–L_phen (**4**) and Zn–D_phen (**5**) based on the emission of the ligand; the experiments run on the rest of the enantiomeric pairs did not yield measurable CPL signal.

To begin with, fluorescence spectra has been collected in the 350–750 nm region; nonetheless, the CPL signal was only clearly detectable at 560–610 nm. This is due to numerous transitions occurring below the fluorescence band and that the transition involved in CPL is only appreciable at high wavelengths and in consequence, low energetic range. Because of that reason, spectra have been recorded in the aforementioned region allowing multiple accumulations to reduce signal noise.

Recorded CPL spectra present weak but distinguished opposed signals (Figure 13). No maxima can be foreseen since the observed region corresponds to the tail of the emission appreciated in the steady-state photoluminescent spectrum which stems from the ligand π-π^* electronic transition.

As observed, in Figure 13, Zn–L_phen (**4**) presents a negative signal meaning that it emits preferentially right-handed circularly polarized emission, while Zn–D_phen (**5**) exhibits major emission of left-handed CPL. As aforementioned, equipment correction error is slightly negative, which triggers g_{lum} values of racemic mixture values being slightly negative. Acquired dissymmetry factor g_{lum} exhibit values around 1×10^{-3}; measuring g_{lum} values for L- 2.38×10^{-3} and D enantiomer 2.22×10^{-4}, respectively. These results confirm that the compound can produce the searched luminescent phenomenon in suspension since the emitted light is similarly polarized in opposite directions by each enantiomer.
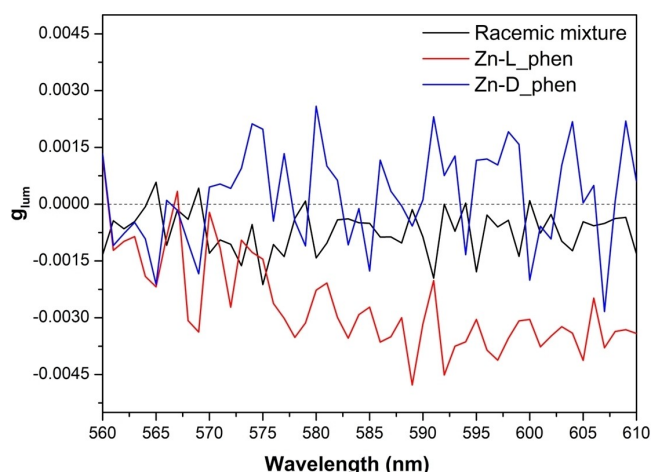

Figure 13. g_{lum} values of the CPL bands were found for the main emission bands of compounds Zn–L_phen (**4**) and Zn–D_phen (**5**).

Nonetheless, to further confirm that obtained weak signals steam from the sample and were not derived from the data-collection procedure, a statistical study was performed according to the procedure described in the bibliography.[47] For this statistical analysis of CPL activity, collected 100 scans recorded for each enantiomer (L- and D-) along with a racemic mixture were divided into 10 sets of scans; then, the mean corresponding to the 10-scan subgroup was calculated and the corresponding average area was determined for each data set. In all cases, to avoid any relationship between the compared sets of data those have been randomized. Figure 14 exhibits represented data, as it can be appreciable, the D-enantiomer displays only positive areas while L- the enantiomer exhibits negative values, which indicates that the net negative areas calculated for the spectra delimit in the negative part of the scale. Racemic mixture shows opposite signed areas.

Subsequently, the mean of the integrated area and its standard deviation were calculated for the spectra of each compound taking into consideration all data sets. With this information, F-test variance and t-test were conducted intend-
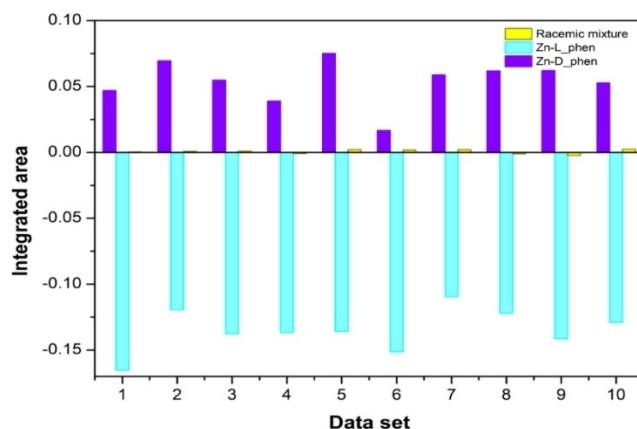

Figure 14. Areas of the differentiated data set were obtained from the CPL activity of compounds Zn–L_phen (**4**, blue) and Zn–D_phen (**5**, purple), and the racemic mixture (yellow).

Table 1. F-test for the area data.

	F_{calc}	F_{tab}
Zn–L_phen (**4**)	100.41	3.18
Zn–D_phen (**5**)	107.99	3.18
$F_{calc} < F_{tab}$		

Table 2. t-test for the area data of the CPL activity of the L and D enantiomers concerning the racemic mixture.

	t_{calc}	t_{tab}
Zn–L_phen (**4**)	26.48	2.10
Zn–D_phen (**5**)	10.02	2.10
$t_{calc} > t_{tab}$		

ing to conclude whether variances significantly differ among them and determine the veracity of the recorded CPL signals. In t-student statistical analysis, a comparison of L- and D-enantiomers data concerning racemic mixture was performed.

The F-test statistical analysis yielded results collected in Table 1. According to results, calculated F values are higher than tabulated ones which determines that according to F-test variances differ significantly in both cases.

Additionally, t-student statistical analysis was carried out as aforementioned with the objective of comparing data obtained for each enantiomer with respect to racemic mixture. The t student analytical analysis results are summarized in Table 2.

Taking into consideration the values of t-student statistical analysis, it was observed that calculated t-student value is higher than the tabulated one which indicates that at 95% confidence signals observed for L- and D- enantiomer are significantly higher compared to racemic mixture signals (ESI, Chiroptical properties, Tables S5–S9). Statistical analysis of the CPL data section. Statistical analysis of the CPL data carried out in samples Zn–L_phen (**4**) and Zn–D_phen (**5**) and the racemic mixture allowed confirming that despite the signal weakness, the collected spectra are derived from the sample and that no error has been performed in the data collection which could detriment recorded data.

Experimental Section

Compound Synthesis

The synthesis of the precursors was carried out according to the procedure described by McKinney et al.[10]

N-(2-Cyanoethyl)glycine: 3.76 g (0.05 mol) of glycine was suspended in 20 mL of deionized water in an Erlenmeyer flask. One equivalent of sodium hydroxide was dissolved in 10 mL of water and added dropwise to the amino acid solution. In this step, it is important to keep the temperature below 30 °C. To the cold alkaline solution, 1.25 equivalents of acrylonitrile were added dropwise and kept stirring for 2 h until a colourless solution was obtained. It is important to notice that temperature may rise while acrylonitrile is being added. That is why acrylonitrile addition to the amino acid solution was done in an ice bath to avoid side reactions which would reduce the yield of the monocyanoethyl derivative. Subsequently, the solution had stood overnight in the fridge. Then, 2.86 mL (0.05 mol) of acetic acid was added to the reaction keeping magnetic stirring. Subsequently, reaction volume was reduced to 10 mL and 50 mL ethanol was added afterwards. After standing overnight in the fridge N-(2-Cyanoethyl)-glycine precipitates and is collected by filtration and washed with ethanol.

N-(2-Cyanolethyl)-L- or -D-valine: The same procedure was used for the cyanoethylation of L- or D-valine. In this case, 2 g (0.017 mol) of L- or D-valine were suspended in 10 mL of deionized water. The addition of one equivalent of NaOH dissolved in 4 mL of H_2O allowed the dissolution of the ligand. As previously described, this step was carried out in an ice bath. Finally, 1.67 mL (0.0255 mol) of acrylonitrile was added keeping the temperature below 30 °C to avoid side reactions left reacting for 2 h. The resulting solution was stood in the fridge overnight before ligand acidification with an equivalent of acetic acid with 1 mL (0.017 mol). Finally, 50 mL of EtOH was added to promote ligand complete precipitation. After standing for an hour in the fridge crystals were collected by filtration and washed with ethanol. The product was recrystallized in hot water.

N-(2-Cyanoethyl)-L- or -D-phenylalanine: For the synthesis of these precursors the procedure followed in the cyanoethylation of glycine was pursued. In this case, 1.65 g (0.1 mol) of L- or D- phenylalanine, 0.6 g (0.015 mol) of NaOH and 1.1 mL (0.0165 mol) of acrylonitrile were used. After the addition of acrylonitrile and standing in the fridge overnight it was necessary to reflux for 2 h to complete de reaction. The acidification process was performed by adding an equivalent of concentrated hydrochloric acid and precipitation occurred instantaneously. After standing in the fridge overnight the precipitate was collected by filtration and washed with water.

N-(2-Cyanoethyl)-L- or -D-tyrosine: It was followed exactly the procedure described for phenylalanine. 2 g (0.01 mol) of L- or D- tyrosine, 0.6 g (0.015 mol) NaOH and 1.1 mL (0.0165 mol) acrylonitrile were used to carry on the reaction.

Transition Metal-Based Compound Synthesis

In general, the synthesis of the complexes was performed by hydrothermal reaction of the appropriate metal chloride or nitrate (1 mmol) with the corresponding N-(2-cyanoethyl)amino acid derivative (1 mmol) and sodium azide (1.5 mmol), in water/methanol solvent mixture (5:5 mL) at 100 °C for 12 h followed by cooling to room temperature over 3 h produced single crystals. Their crystal structures were determined using single crystal X-ray crystallography. In the succeeding lines a detailed procedure will be described for each compound:

Synthesis of Single Crystals of $[Mn_2L^1_2(H_2O)_4]\cdot H_2O$, in Advance Mn_gly (1)

0.128 g (1 mmol) of N-(2-cyanoethyl)glycine precursor were dissolved in 5 mL of an equal mixture of H_2O/MeOH, 0.065 g (1 mmol) of NaN_3 was added to the solution and 0.198 g (1 mmol) of $Mn(NO_3)_2 \cdot 4H_2O$. The solution was placed in a Teflon liner vessel and heated at 100 °C for 12 h. Single crystals were obtained after cooling down to room temperature.

Chemistry–A European Journal

Research Article
doi.org/10.1002/chem.202304146

Chemistry Europe
European Chemical
Societies Publishing

Synthesis of Single Crystals of [ZnL²]ₙ, in Advance Zn-L/D_val (2/3)

0.26 g of (1.5 mmol) of N-(2-cyanoethyl)-L or D-valine derivative were dissolved in 10 mL water/5 mL methanol mixture. To this solution, first 0.129 g (1.98 mmol) of NaN_3 were added and once dissolved, 0.45 g (1.5 mmol) of $Zn(NO_3)_2\cdot 6H_2O$. Magnetic stirring was kept for 10 minutes and the colourless solution was placed in a capped vial and placed at 100 °C for 12 h to get single crystals.

Synthesis of Single Crystals of [ZnL³]ₙ, in Advance Zn-L/D_phen (4/5)

0.22 g of (1 mmol) of N-(2-cyanoethyl)-L- or -D-phenylalanine derivative were suspended in a mixture of 10 mL H_2O/5 mL MeOH. 0.04 g (1 mmol) of NaOH were added to the suspension to get a dissolution to which 0.065 g (1 mmol) of NaN_3 were added. Finally, 0.30 g (1 mmol) of $Zn(NO_3)_2\cdot 6H_2O$ to the reaction and kept stirring for 10 minutes. The final solution was poured into a capped vial and placed in the oven for 12 h at 100 °C. Single crystals were obtained after slowly cooling down to room temperature.

Synthesis of Single Crystals of {[ZnL⁴]·H₂O}ₙ, in Advance Zn-L/D_tyr (6/7)

The same procedure was followed for the synthesis of Zn–L/D_phen (**4/5**), but in this case, 0.234 g (1 mmol) of N-(2-cyanoethyl)-L- or -D-tyrosine precursor were used for the reaction.

Synthesis of {[CdL⁴]·H₂O}ₙ, in Advance Cd-L/D_tyr (8/9)

0.117 g (0.5 mmol) of N-(2-cyanoethyl)-L- or -D-tyrosine precursor, 0.154 g (0.5 mmol) of $Cd(NO_3)_2\cdot 4H_2O$ and 0.0325 g (0.5 mmol) of NaN_3 were weighted in a vial. 8 mL of water were added and placed in a Teflon liner vessel solvothermal reactor for 48 h at 140 °C. After slow cooling to room temperature, the polycrystalline powder was obtained, which was collected by filtration and washed with water.

The corresponding structural characterization (elemental analysis, FTIR spectra and PXRD) was performed for all compounds to confirm the purity of the samples. For more details see the ESI (Tables S10–S14 and Figures S1–S7).

UHPLC/Q-TOF-MS Measurements

All UHPLC/Q-TOF-MS data were acquired on a SYNAPT G2 HDMS, coupled to a quadrupole time of flight (Q-ToF) configuration (Waters) equipped with an ESI source operating in positive and negative ion modes. The spectra were acquired over the 50–1200 m/z range and automatically corrected during acquisition using the lock mass with leucine encephalin solution (2 ng/μL) in methanol:water (50:50, v/v) and 0.1% formic acid. The reference internal standards were introduced into the lock mass sprayer at a constant flow rate of 10 μL/min using an external pump.

Dynamic Light Scattering Measurements

The particle size and zeta potential were also evaluated by a dynamic light scattering technique with a Malvern Zetasizer ZS equipment (Malvern Panalytical, Malvern, UK). The dried powder samples were dispersed in distilled water in 0.5 mM concentration, and the dispersion was sonicated for 10 minutes. All measurements were made at room temperature and shown values are the average of 9—12 replicates.

Relaxation Time Measurements

Relaxativity measurements were carried out in compound **1** (Mn_gly). For that purpose, solutions of 1 mM, 0.5 mM and 0.1 mM concentration (relative to Mn^{2+}) were prepared in Milli-Q water and analysed. To ensure that the material was completely dissolved, they were sonicated over 30 minutes and filtered off by a 0.22 μm microfilter. Milli-Q water employed in dissolution preparation was used as blank or reference in relaxativity measurements. Three different measurements of T_1 and T_2 were performed for each sample and each concentration. Relaxivity values r_1 and r_2 were obtained from the slopes of the curves $1/T_1$ and $1/T_2$ vs. the concentration of Mn^{2+} expressed in mM.

Chiroptical Properties

General Procedure for Circular Dichroism Experiments

Samples for CD measurements were prepared as follows: a precision weighted amount of material (2 mg) was suspended in Milli-Q H_2O (4 mL) and sonicated over 1 h.

General Procedure for Circularly Polarized Luminescence Experiments

Samples for CPL measurements were prepared as follows: a precision weighted amount of well-grounded material (5 mg) was suspended in 4 mL H_2O and sonicated over 5 min. To prevent material decantation sample was manually shacked between spectra collection. For racemic mixture preparation, well-grounded 2.5 mg of L-enantiomer and 2.5 mg of D-enantiomer were weighed and suspended in 4 mL of H_2O. Next, fluorescence and CPL spectra were collected for pure enantiomers. The resulting CPL spectra were calculated as an average of recorded 100 scans.

For data collection, a set of 100 scans for each enantiomer and the racemic mixture have been recorded in suspension exciting the sample by 300 nm LED. Note that, the equipment possesses a negative correction.

As a proof of concept, and to ensure that the material remains stable in water, 5 mg of material were suspended in 4 mL of H_2O and sonicated for 5 minutes. Then, the decanted solution was filtered with the aid of a 45 μm syringe and fluorescence and CPL of the solution were collected giving in all enantiomeric pairs a negligible CPL and luminescence signal.

Statistical Analysis of the Chiroptical Properties

F-test variance and t-test were conducted intending to conclude whether variances significantly differ among them and determine the veracity of the recorded CPL signals. In t-student statistical analysis, a comparison of L- and D- enantiomers data concerning racemic mixture was performed.

Conclusions

In this work, we have successfully synthesised and characterized a family of nine multifunctional coordination compounds based on (2-(1H-tetrazol-5-yl)ethyl)amino acid derivative (amino acid = glycine, valine, phenylalanine and tyrosine) ligands and d-block metals. Concretely, relaxativity measurements have been carried out in Mn^{2+} based compound **1**, being a novel manganese-

Chemistry–A European Journal

Research Article
doi.org/10.1002/chem.202304146

Chemistry Europe
European Chemical
Societies Publishing

based contrast agent which could find potential application in magnetic resonance imaging as a T_2 contrast agent. The high r_2/r_1 ratio, along with observed signal intensity reduction and endarkening found in T_2-weighted images has prompted us to conclude compound **1** potential applicability as a T_2 contrast agent. Future research steps should be conducted in the direction of **1** being clinically applied. For that purpose, future analysis will address additional characteristics such as its cytotoxicity, aggregation of blood proteins and biodistribution and pharmacokinetics with *in vivo* experiments. On another level, motivated by the extended aromaticity of *in situ* synthesised ligands, photoluminescent properties have been studied in d^{10} metal derived complexes. Compounds **6–9** display similar excitation and emission lines derived from ligand centred $\pi\rightarrow\pi^*$ transition emission in all cases displaying relatively short decay times of around 5 ns. Finally, amino acid precursor's preserved chirality prompted us to study the chiroptical properties of compounds **6–9**. Circular dichroism allowed us to conclude that in all cases enantiomeric pairs display opposite cotton effects being only Zn_phen enantiomeric pairs able to display circularly polarized luminescence. Obtained dissymmetry factor, g_{lum}, is in the range of 1×10^{-3} and line with values examples in the bibliography. To conclude, we further confirmed by statistical study that the obtained weak CPL is a property intrinsic to the sample and does not derive from the data-collection procedure.

Supporting Information

The authors have not cited additional references within the Supporting Information.

Acknowledgements

Conflict of Interests

The authors declare no conflict of interest.

Data Availability Statement

CCDC 2332735–2332740 contain the supplementary crystallographic data for this paper, which are provided free of charge by the Cambridge Crystallographic Data Centre.

[1] X. M. Chen, M. L. Tong, *Acc. Chem. Res.* **2006**, *40*, 162–170.
[2] X. M. Zhang, *Coord. Chem. Rev.* **2005**, *249*, 1201–1219.
[3] Z. P. Demko, K. B. Sharpless, *J. Org. Chem.* **2001**, *66*, 7945–7950.
[4] Z. P. Demko, K. B. Sharpless, *Org. Lett.* **2002**, *4*, 2525–2527.
[5] Z. P. Demko, K. B. Sharpless, *Org. Lett.* **2001**, *3*, 4091–4094.
[6] S. Vorona, T. Artamonova, Y. Zevatskii, L. Myznikov, *Synth.* **2014**, *46*, 781–786.
[7] D. Cantillo, B. Gutmann, C. O. Kappe, *J. Am. Chem. Soc.* **2011**, *133*, 4465–4475.
[8] I. A. Shikhova, T. A. Sinitsyna, M. I. Ermakova, N. I. Latosh, *Zh. Obshch. Khim.* **1985**, *55*, 2374–2377.
[9] L. L. Mckinney, E. A. Setzkorn, E. H. Uhing, *J. Am. Chem. Soc.* **1952**, *74*, 3–4.
[10] W. G. Finnegan, R. A. Henry, R. Lofquist, *J. Am. Chem. Soc.* **1958**, *80*, 3908–3911.
[11] L. L. McKinney, E. H. Uhing, E. A. Setzkorn, J. C. Cowan, *J. Am. Chem. Soc.* **1950**, *72*, 2599–2603.
[12] M. Nasrollahzadeh, Z. Nezafat, N. S. S. Bidgoli, N. Shafiei, *J. Mol. Catal.* **2021**, *513*, 111788.
[13] C. X. Wei, M. Bian, G. H. Gong, *Mol.* **2015**, *20*, 5528–5553.
[14] S. I. Elewa, N. A. Fatthallah, M. I. Nessim, A. F. El-Farargy, *Arab. J. Chem.* **2020**, *13*, 8750–8757.
[15] V. A. Ostrovskii, R. E. Trifonov, E. A. Popova, *Izv. Akad. Nauk Ser. Khim.* **2012**, *61*, 765–0777.
[16] E. A. Popova, R. E. Trifonov, V. A. Ostrovskii, *Russ. Chem. Rev.* **2019**, *88*, 644–676.
[17] A. Salinas-Castillo, A. J. Calahorro, D. Briones, D. Fairen-Jiménez, F. Gándara, C. Mendicute-Fierro, J. M. Seco, M. Pérez-Mendoza, B. Fernández, A. Rodríguez-Diéguez, *New J. Chem.* **2015**, *39*, 3982–3986.
[18] Y. Xu, W. Liu, D. Li, H. Chen, M. Lu, *Dalton Trans.* **2017**, *46*, 11046–11052.
[19] a) A. J. Calahorro, A. Salinas-Castillo, J. M. Seco, J. Zuñiga, E. Colacio, A. Rodríguez-Diéguez, *CrystEngComm* **2013**, *15*, 7636; b) W. Shuai-Hua, Z. Fa-Kun, Z. Ming-Jian, L. Zhi-Fa, C. Jun, X. Yu, W. A-Qing, G. Guo-Cong, H. Jin-Shun, *Inorg. Chem.* **2013**, *52*, 10096–10104.
[20] A. Rodríguez-Diéguez, A. J. Mota, J. M. Seco, M. A. Palacios, A. Romerosa, E. Colacio, *Dalton Trans.* **2009**, 9578–9586.
[21] S. Lacerda, *Inorganics* **2018**, *6*, 1–17.
[22] D. Pan, A. H. Schmieder, S. A. Wickline, G. M. Lanza, *Tetrahedron* **2011**, *67*, 8431–8444.
[23] A. I. Martínez-Banderas, A. Aires, S. Plaza-García, L. Colás, J. A. Moreno, T. Ravasi, J. S. Merzaban, P. Ramos-Cabrera, A. L. Cortajarena, J. Kosel, *J. Nanobiotechnol.* **2020**, *18*, 1–12.
[24] B. N. Siriwardena-Mahanama, M. J. Allen, *Molecules* **2013**, *18*, 9352–9381.
[25] J. Wang, H. Wang, I. A. Ramsay, D. J. Erstad, B. C. Fuchs, K. K. Tanabe, P. Caravan, E. M. Gale, *J. Med. Chem.* **2018**, *61*, 8811–8824.
[26] H. Liu, X.-A. Zhang, *Encycl. Inorg. Bioinorg. Chem.* **2018**, 1–16.
[27] J. Wahsner, E. M. Gale, A. Rodríguez-Rodríguez, P. Caravan, *Chem. Rev.* **2019**, *119*, 957–1057.
[28] P. C. Lauterbur, *Nature.* **1973**, *242*, 190–191.
[29] K. Leyba, B. Wagner, *Curr. Opin. Nephrol. Hypertens.* **2019**, *28*, 154–162.
[30] A. Barbieri, G. Accorsi, N. Armaroli, *Chem. Commun.* **2008**, 2185–2193.
[31] E. San Sebastian, A. Rodríguez-Diéguez, J. M. Seco, J. Cepeda, *Eur. J. Inorg. Chem.* **2018**, 2155–2174.
[32] J. Cepeda, E. San Sebastián, D. Padro, A. Rodríguez-Diéguez, J. A. García, J. M. Ugalde, J. M. Seco, *Chem. Commun.* **2016**, *52*, 8671–8674.
[33] Y. Cui, Y. Yue, G. Qian, B. Chen, *Chem. Rev.* **2012**, *112*, 1126–1162.
[34] E. M. Sánchez-Carnerero, A. R. Agarrabeitia, F. Moreno, B. L. Maroto, G. Muller, M. J. Ortiz, S. De La Moya, *Chem. A Eur. J.* **2015**, *21*, 13488–13500.
[35] Y. Sang, J. Han, T. Zhao, P. Duan, M. Liu, Y. Sang, M. Liu, T. Zhao, P. Duan, J. Han, *Adv. Mater.* **2020**, *32*, 1900110.
[36] R. Singh, K. N. Narayanan Unni, A. Solanki, *Opt. Mater.* **2012**, *34*, 716–723.
[37] M. C. Heffern, L. M. Matosziuk, T. J. Meade, *Chem. Rev.* **2013**, *114*, 4496–4539.
[38] M. Llunell, D. Casanova, J. Cirera, J. M. Bofill, P. Alemany, S. Alvarez, M. Pinsky, D. Avnir, *Program for the Stereochemical Analysis of Molecular Fragments by Means of Continuous Shape Measures and Associated Tools. SHAPE, v1.1b, Barcelona, Spain* **2005**, 1–35.
[39] V. A. Blatov, A. P. Shevchenko, D. M. Proserpio, *Cryst. Growth Des.* **2014**, *14*, 3576–3586.
[40] R. K. Mudsainiyan, A. K. Jassal, S. K. Chawla, *J. Solid State Chem.* **2015**, *230*, 61–69. https://doi.org/10.1016/J.JSSC.2015.04.001.
[41] P. Caravan, C. T. Farrar, L. Frullano, R. Uppal, *Contrast Media Mol. Imaging* **2009**, *4*, 89–100.

Chem. Eur. J. **2024**, *30*, e202304146 (11 of 12)

© 2024 The Authors. Chemistry - A European Journal published by Wiley-VCH GmbH

[42] M. Regueiro-Figueroa, G. A. Rolla, D. Esteban-Gómez, A. De Blas, T. Rodríguez-Blas, M. Botta, C. Platas-Iglesias, *Chem. A Eur. J.* **2014**, *20*, 17300–17305.

[43] B. Phukan, C. Mukherjee, U. Goswami, A. Sarmah, S. Mukherjee, S. K. Sahoo, S. C. Moi, *Inorg. Chem.* **2018**, *57*, 2631–2638.

[44] P. Boraschi, F. Donati, R. Gigoni, D. Caramella, U. Boggi, F. Falaschi, C. Bartolozzi, *Eur. Radiol.* **2006**, *16*, 988–997.

[45] J. Cepeda, A. Rodríguez-Diéguez, *CrystEngComm* **2016**, *18*, 8556–8573.

[46] P. Li, Z. Zhou, Y. S. Zhao, Y. Yan, *Chem. Commun.* **2021**, *57*, 13678–13691.

[47] P. Leo, G. Orcajo, J. A. García, A. M. Ortuño, J. M. Cuerva, D. Briones, G. Calleja, A. Rodríguez-Diéguez, R. Sanz, J. Cepeda, F. Martínez, *J. Mater. Chem. C* **2021**, *9*, 5544–5553.